Article

Research on the Device of Micro Droplet PCR in Microfluidic Chip Based on Constant Pressure Regulation

Luyang Duanmu [1], Yuanhua Yu [1,2,*] and Xiangkai Meng [2]

[1] School of Physics, Changchun University of Science and Technology, Changchun 130022, China;1044384096@qq.com (L.D.); Yhycust@163.com (Y.Y.)
[2] School of Life Science and Technology, Changchun University of Science and Technology, Changchun 130022,China; Yhycust@163.com (Y.Y.); mxk2018@cust.edu.cn (X.M.)
* Correspondence: yuyuanhua8888@126.com

Abstract: The device and method in accordance with the constant pressure regulation of micro droplet PCR in microfluidic chips are developed to explore the optimization way for the micro droplet movement, fragmentation, and bubble generation in microfluidic chips in existing digital PCR technology. In the developed device, an air source device is adopted to regulate the pressure in the chip, such that micro droplet generation and PCR amplification without bubbles can be achieved. In 3 min, the sample in 20ul will be distributed into nearly 50,000 water-in-oil droplets exhibiting a diameter of about 87μm, and the micro droplet will be subjected to a close arrangement in the chip without air bubbles. The device and chip are adopted to quantitatively detect the human gene . As indicated by the experimental results, a good linear relationship exists between detection signal and DNA concentration ranging from 10^1~ 10^5 copies /μL (R2=0.999). The micro droplet PCR devices based on constant pressure regulation chips exhibit a wide variety of advantages (e.g., achieving high pollution resistance, micro droplet fragmentation and integration avoidance, reducing human interference, and standardizing results). Thus, micro droplet PCR devices based on constant pressure regulation chips have promising applications in nucleic acid quantification.

Keywords: Constant Pressure Regulation; Micro droplet Digital PCR; Fluorescence Detection; Quantitative Detection

1. Introduction

Polymerase Chain Reaction (PCR), highlighted by widespread application in genetic analysis and disease diagnosis, has aroused wide attention and research interest over the past few years [1-3]. Based on the digital PCR developed from microfluidic technology, the latest generation of PCR technology is of smaller reaction volume, faster reaction speed, lower system noise, and higher sensitivity than that of conventional qPCR. Digital PCR can currently fall into two types, i.e., Type I and Type II. To be specific, Type I allocates nucleic acids into discrete micropores or microchambers, and Type II dilutes the target into considerable independent uniform picoliter or nanoliter droplets [4]. In general, Type II, droplet digital PCR (ddPCR), is capable of achieving higher reaction volumes at lower costs than that of the former. Digital Polymerase Chain Reaction (PCR) amplifies separated targets in numerous microreactors and applies Poisson statistics to quantify DNA concentration. Kinzler and Vogelstein et al. for the first time reported the principle of digital PCR [2]. Featured with its superior characteristics (e.g., absolute quantification of nucleic acid, higher reproducibility than real-time PCR, and lower susceptibility to inhibition), the strength tool has been extensively employed to investigate circulating tumor DNA [5], copy number variation [6], gene expression [7], rare mutation detection[8], single cell analysis [9, 10], and trace nucleic acid detection [11].

It is worth noting that stabilizing considerable monodisperse droplets is of high challenge for ddPCR applications. Droplets must withstand critical conditions throughout the entire PCR process, including the rapid temperature cycling and complex aqueous

Preprints (www.preprints.org) | NOT PEER-REVIEWED | Posted: 30 May 2023 doi:10.20944/preprints202305.2110.v1

samples [12]. Accordingly, there are several key issues that limit the further application of ddPCR, including bubble generation and evaporation. For the evaporation, it's applicable to use oil seals for solving [13]. However, how to deal with the generation of bubbles is still being actively explored. The formation of bubbles is a common cause of microfluidic issue and one of the main reasons for PCR failure on chips [14].

There are existed bubbles and newly generated bubbles in the ddPCR process, including bubbles mixed from the sample [15] and residual microbubbles in the gaps of the chip microstructure [16]. The newly generated bubbles are mainly generated during the rapid heating and cooling process of PCR, since the decreased gas solubility of oil under high temperature conditions, resulting in the formation of bubbles during oil degassing [17]. In the heating process, the bubbles mixed into the droplets are likely to move, gather, and grow, move the lotion out of the reaction chamber, or apply a shear force on the droplets, thus triggering the droplet integration and problems in the reading process, such that the performance and outcome of the entire PCR can be determined [17]. Indeed, the insufficiencies of bubbles have been recognized by the society, and some studies have been conducted on bubbles removal. The bubble removal mechanism in microsystems conforms to membranes, porous structures, capillary interactions and/or diffusion, and the application of vacuum in the past, as reviewed by Xu et al. [18, 19]. The above-mentioned methods ensure the PCR process by eliminating bubbles, whereas there are numerous challenges (e.g., the complex and cumbersome processes failed to industrialize on a large scale and to apply subsequent fluorescence detection).

To address the above-mentioned problems, a novel constant pressure control device is proposed in this study that employs positive pressure injection to generate micro droplets at the micro droplet generation stage. Moreover, in the PCR process, the method of constant pressure regulation of micro droplets in microfluidic chips is adopted to suppress the precipitation and growth of bubbles, such that the stability of micro droplets can be enhanced. The device achieves micro droplet generation, PCR amplification, and chip fluorescence signal reading on the identical chip, avoiding the effect of bubbles in the experimental process. In addition, the performance of the chip based constant pressure regulatory device in nucleic acid quantitative detection is verified by detecting the Epidermal Growth Factor Receptor (EGFR) gene, which can serve as a molecular indicator for early detection of mutated DNA. The detection of DNA mutations can serve as a molecular indicator for early detection of tumors and can also provide guidance for the use of molecular targeted therapies [20]. Thus, the study of droplet PCR devices in constant pressure regulated microfluidic chips provides guidance for the in-depth practical application of droplet digital PCR chips.

2. Materials and Methods

2.1 . Reagents and Instruments

Droplet generation oil (biological level), forward primers, reverse primers, MGB probes, pGEM plasmids embedded in EGFR exon gene 18 sequence, ddPCRSupermix for Probes; ddPCR gene chip reader, Manta g-1236 CMOS camera, 200uL centrifuge tube (AXYGEN), micropipette (Eppendorf), suction head (AXYGEN), handheld centrifuge (Eppendorf), pressure calibrator, temperature calibrator, Peltier, flexible trachea, aluminum plate, PT1000, TM115 temperature control module, 42 stepper motor, sealed through hole rubber plug; ultra clean workbench, silicon wafer, photoresist SU-8 (Micro Chem 2050), cyclic olefin copolymer (TOPAS 5031), (tridecafluoro-1,1,2,2,2-tetrahydrooctyl) trichlorosilane (United Chemical Technologies, Inc., Bristol, PA), dryer, UV lamp, desktop homogenizer, incubator, plasma cleaning machine, proportional valve, MFS flow sensor, as well as solenoid valve. ImageJ software is adopted to process images captured in experiments.

2.2. Design and Fabrication of the Integrated Ddpcr Gene Chip

Preprints (www.preprints.org) | NOT PEER-REVIEWED | Posted: 30 May 2023 doi:10.20944/preprints202305.2110.v1

Fig. 1 presents the composition and working principle of the ddPCR integrated gene chip through research, which achieves droplet generation, PCR amplification, and fluorescence signal reading on the identical chip.

The integrated ddPCR gene chip comprises two parts, droplet generation and droplet collection chamber. Solidworks software is employed to design the integrated chip structure diagrams. Microfluidic chips are manufactured using the conventional photolithography methods [21-25] and COC injection molds. The design of the microfluidic chip is illustrated in Fig. 1. The main mold of the equipment is manufactured using the conventional SU8 lithography process. After the development process, the main mold is hard functionalized at 150 ° C for 30 min and salted with (tridecafluoro-1,1,2,2-tetrahydrooctyl) trichlorosilane (United Chemical Technologies, Inc., Bristol, PA) for 5 min to prevent pattern removal during polymer replication (Fig. 2a). Subsequently, the COC particles are placed into the injection molding machine (CT80M8), the mold temperature is set to 60 ° C, the melt temperature is set to 215 ° C, the injection speed is set to 97mm/s, the injection pressure is set to 60MPa, and the pressure setting is kept at 60mPa. The molten COC enters the mold under the push of the screw, and the chip structure layer with microchannel structure is obtained after cooling (Fig. 2b). Live tissue is adopted to inspect punch holes with a diameter of 1mm. The preparation of COC chips can be achieved by hot pressing and bonding the chip structure layer with another COC plastic sheet after oxygen plasma treatment (PDC-MG, Harris plasma) for 1 minute and baking for 6 min (Fig. 2c. d). The chip is placed in an oven at 105 ° C for 5 h after the production is achieved to enhance the hydrophobicity of the inner wall of the microchannel and ensure the stability of the droplets. The real chip is illustrated in Fig. 2.e.

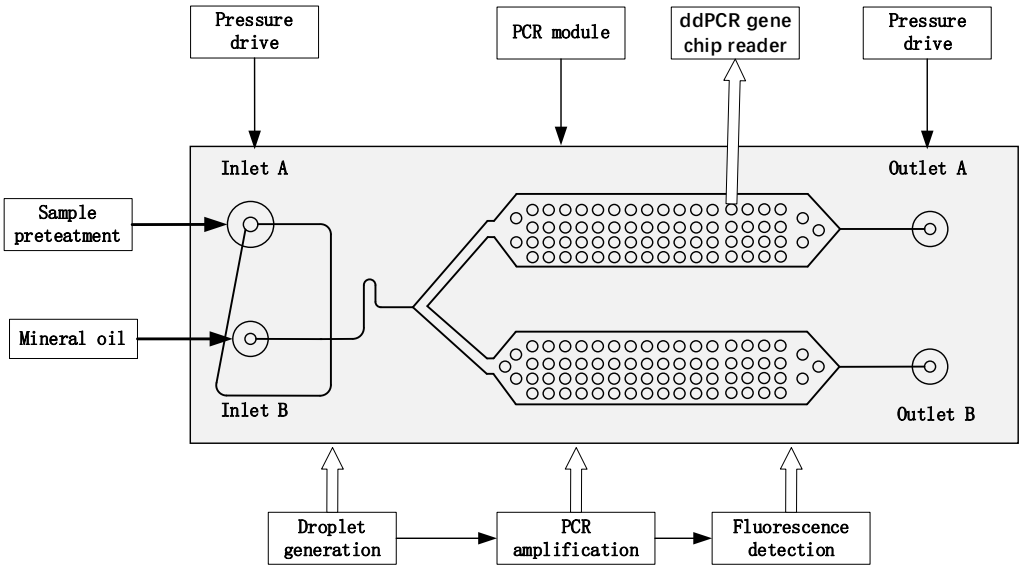

Figure. 1 Layout of the integrated droplet digital polymerase chain reaction (ddPCR) gene chip for droplet generation, collection, on chip thermal cycling, and fluorescence readout

Preprints (www.preprints.org) | NOT PEER-REVIEWED | Posted: 30 May 2023 doi:10.20944/preprints202305.2110.v1

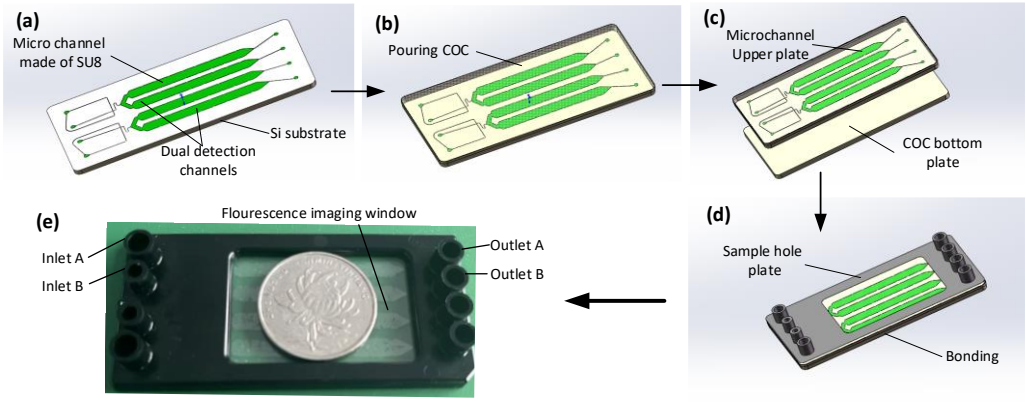

Figure. 2 Fabrication process of the integrated droplet digital polymerase chain reaction (ddPCR) gene chip. Mold manufactured by photolithography (a). Pouring cyclic olefin copolymer (COC) (b). Bonding (c). Sketch of the chip (d). Image of the chip (e)

2.3 Methods

2.3.1. Bubble dynamics equation

Bubble dynamics mainly studies the dynamic growth or reduction of bubbles in liquids. The Rayleigh Plesset equation is a classic equation that describes the dynamic changes of bubbles, and its derivation assumption is:

1. The liquid is incompressible Newtonian fluid;
2. Gravity can be ignored;
3. The gas in the bubble is composed of liquid vapor and non-condensable gas. The liquid vapor in the bubble is in a saturated state, and its partial pressure is the saturated vapor pressure. The non-condensing gas content in the bubble is constant;
4. The inertia of gas and the heat exchange between gas and liquid can be ignored.

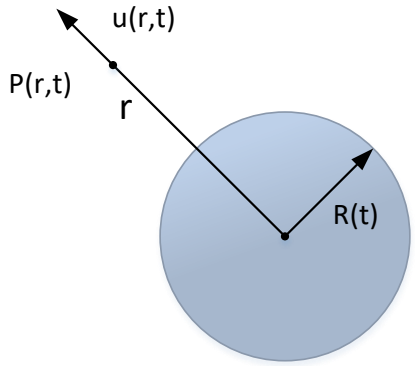

Figure 3. Bubble diagram

The spherical coordinates with the center of the bubble as the origin are set, as presented in Figure. During the bubble change, R (t) denotes the radius of the bubble. P (r, t) denotes the pressure at any point r in the liquid, and u (r, t) expresses the velocity, such that the equation Rayleigh Plesset can be deduced to express the dynamic behavior of bubbles as:

$$\rho\left(R\ddot{R}+\frac{3}{2}\dot{R}^2\right)=P_v-P_f(t)+P_{g0}\left(\frac{R_0}{R}\right)^3-\frac{2\sigma}{R}-4\mu_0\frac{\dot{R}}{R} \quad (1)$$

2.3.2. Dissolution and precipitation of gases in liquids

When the Rayleigh Plesset equation is being derived, the gas content in the bubble is assumed to be constant. For practical gas-liquid two-phase fluids, gases generally exist in

Preprints (www.preprints.org) | NOT PEER-REVIEWED | Posted: 30 May 2023 doi:10.20944/preprints202305.2110.v1

liquids in two forms. To be specific, Form I is suspended in the form of bubbles in the liquid; Form II dissolves into the liquid. Accordingly, the Rayleigh Plesset equation ignores the effect of gas dissolution and precipitation on bubble dynamics. In addition, the dissolution of gas also affects the steady-state radius of bubbles when the pressure changes.

Henry's law describes the equilibrium state of dissolution. When dissolution equilibrium occurs, the solubility of a gas is directly proportional to the pressure of the gas on the liquid surface.

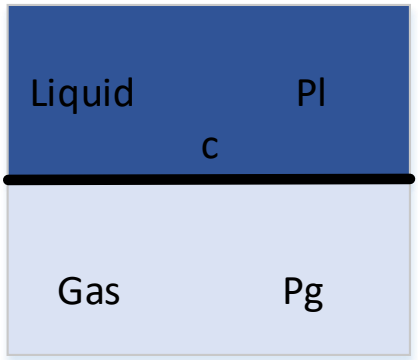

Figure 4. Schematic diagram of diffusion equilibrium at gas-liquid interface

As depicted in Figure. 4, the gas pressure P_g is directly proportional to the solubility c of gas in liquid, where:

$$c = \frac{P_g}{H} \tag{2}$$

Where H is the Henry constant.

When calculating the effect of gas dissolution on the evolution of bubble radius, it is necessary to clarify the diffusion law of gas between bubbles and liquids. Fick's diffusion law is a macroscopic law that describes the phenomenon of material diffusion, representing that the direct ratio between the flow rate of diffusing substances per unit cross-sectional area perpendicular to the diffusion direction per unit time and the concentration gradient of diffusing substances at the interface. Fick's diffusion law can be expressed as:

$$J_D = -D_g \frac{\partial c}{\partial r} \tag{3}$$

Where J_D denotes the diffusion flow density, with unit of $Kg/m^2 \cdot s$; D_g represents the diffusion coefficient, with unit of m^2/s; c expresses the concentration of gas in the liquid, with the unit of Kg/m^3.

The diffusion coefficient in Eq. 3 can be approximately functioned as temperature and pressure in the bubble.

$$D_g = \frac{2.256}{P_g}\left(\frac{T}{256}\right)^{1.81} \tag{4}$$

2.3.3. Bubble dynamics equation based on diffusion

There is a limited effect of steam in the bubble on the dynamic process of bubbles containing non-condensable gases. Thus, assuming that the bubble is filled with non-condensing gas and does not contain liquid vapor, where:

$$P_v = 0 \tag{5}$$

Where there will be no continuously dissolved or precipitated gases in the practical solution. Accordingly, it is assumed that there is a limited area around the bubble that is capable of affecting gas diffusion or dissolution, where

Preprints (www.preprints.org) | NOT PEER-REVIEWED | Posted: 30 May 2023 doi:10.20944/preprints202305.2110.v1

$$\rho\left(R\ddot{R}+\frac{3}{2}\dot{R}^2\right)=P_g-P_f-\frac{2\sigma}{R}-4\mu_0\frac{\dot{R}}{R} \tag{6}$$

$$\frac{dP_g}{dt}=\frac{3}{R}\left[-R^*T\frac{2.256\left(\frac{P_g}{H_m}-c_r\right)}{M_gP_g\Delta r}\left(\frac{T}{156}\right)^{1.81}-P_g\dot{R}\right] \tag{7}$$

$$\frac{dP_g}{dt}=\frac{3}{R}\left[-R^*T\frac{2.256\left(\frac{P_g}{H_m}-c_r\right)}{M_gP_g\Delta r}\left(\frac{T}{156}\right)^{1.81}-P_g\dot{R}\right] \tag{7}$$

2.4. Constant Pressure Control Device

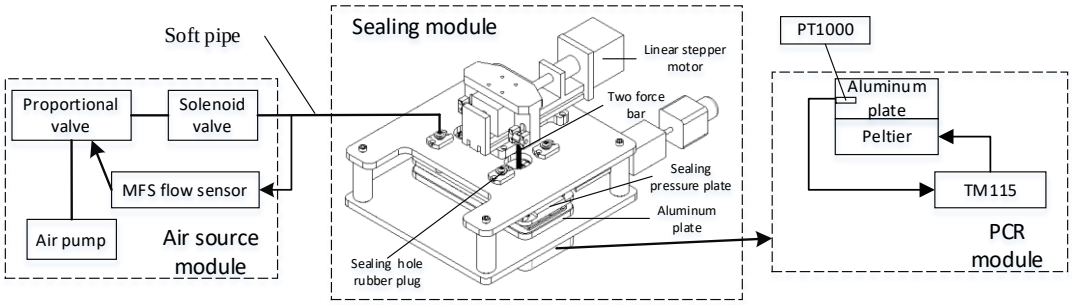

Figure 5. Schematic diagram of constant pressure control device

5 presents the schematic diagram of the experimental device, comprising the PCR module, the sealing module, and the gas source module.

The PCR module provides the rapid temperature variation for nucleic acid sample amplification, which primarily comprises a heating module and a temperature control module. The heating module covers two Parcel patches placed side by side on the aluminum plate, and the two Parcel patches are connected to the power supply in series. Moreover, the temperature control module employs the TM115 module of Chengdu Yexian Technology. In the above module, PT1000 is adopted to collect the temperature of aluminum plates. On the basis of proportional integral (PID) closed-loop control, this module is capable of generating rapid rise and fall and uniform temperature, such that the surface temperature uniformity of aluminum blocks is achieved within ± 0.3 ℃.

The sealing module drives the sealing pressure plate for sealing the microfluidic chip, primarily comprising a sealing pressure plate, a two force rod, a linear stepper motor, and four sealing through-hole rubber plugs. The sealing through-hole rubber plug is connected to the air source module through a flexible gas pipe, and driven by a linear actuator, the sealing pressure plate is pressed down. Thus, the sealed through-hole rubber plug is tightly attached to the inlet and outlet of the chip, ensuring the airtightness of the gas path during droplet generation and PCR.

The air source module provides stable pressure for droplet generation and PCR (e.g., an air pump, MFS flow sensor, a proportional valve, and a solenoid valve). The module can generate stable air pressure through proportional integral (PID) closed-loop control, and the fluctuation range of droplet formation only reaches ± 0.1 millibar. The chip fixture is adopted to fix the droplet generation chip, and it is capable of adjusting the air pressure through a potentiometer. When the instrument operates continuously for 2 h, the fluctuation falls into a scope of ± 1 millibar.

2.5. Data Acquisition and Analysis

After amplification, the PCR transfers the chip to a gene chip image reader for observation. Stimulated by 485nm (FAM) excitation, the fluorescence microscope imaging

Preprints (www.preprints.org) | NOT PEER-REVIEWED | Posted: 30 May 2023 doi:10.20944/preprints202305.2110.v1

system and CMOS image sensor are employed to take photos for capturing the fluorescence images of PCR reaction results. Moreover, ImageJ software is applied to count the number of positive droplets and total droplets [26]. According to Poisson's statistical principle, the absolute amount of target DNA contained in the respective reaction can be calculated using Eq. (1) and the practical number of positive droplets [27]:

$$c = -\frac{\left[n \times \ln\left(1 - {}^{d}/_{n}\right)\right]}{V_d \times n} \tag{9}$$

Where c is the concentration of target DNA in the sample, n is the total number of droplets in the chip, d is the number of positive droplets, V_d is the volume of each droplet.

3. Results and Discussion

3.1. Micro Droplet Generation and Collection

Fig. 6 (b) presents the flow focusing structure generated by liquid droplets. The oil phase wraps the sample into droplets at the intersection of the flow focusing structure and under the combined action of surface tension and shear force. The chip adopts a positive pressure injection method, and the droplet diameter is primarily determined by the size of the flow focusing structure and the flow rate ratio of the discrete phase (sample) to the continuous phase (oil). Furthermore, the droplets generated in the collection chamber are arranged in a single layer.

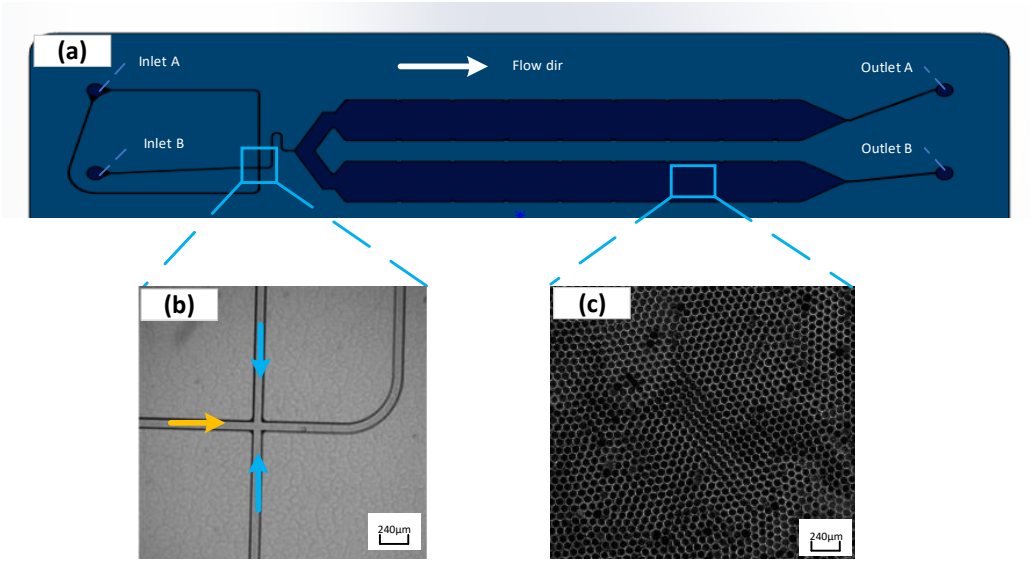

Figure 6. Schematic diagram of the integrated droplet digital polymerase chain reaction (ddPCR) gene chip structure (a). Flow focus structure of droplets generation part (Blue arrows represent the flow direction of the oil; orange arrow represents the flow direction of sample) (b). Single layer arrangement of droplets in the collection chamber (c) (color figure online)

This study highlights how to achieve micro droplets with a diameter of 80 ± 10um. The microchannel size is confirmed to be square in cross-section and in size of 80um × 80um. Prior to the droplet generation, the generated oil is applied to wet the entire flow channel, which is conducive to reducing bubbles in the chip flow channel. Subsequently, 20ul of sample and 70ul of oil are introduced to the chip sampling hole, and the pressures at the oil inlet and sample inlet are set to 161mbar and 273mbar, respectively. The pressure calibrator is adopted to verify the set air pressure of the device, and the results are presented in Fig. 7, suggesting that the pressure falls into a scope of the set ± 0.3 mbar.

Preprints (www.preprints.org) | NOT PEER-REVIEWED | Posted: 30 May 2023 doi:10.20944/preprints202305.2110.v1

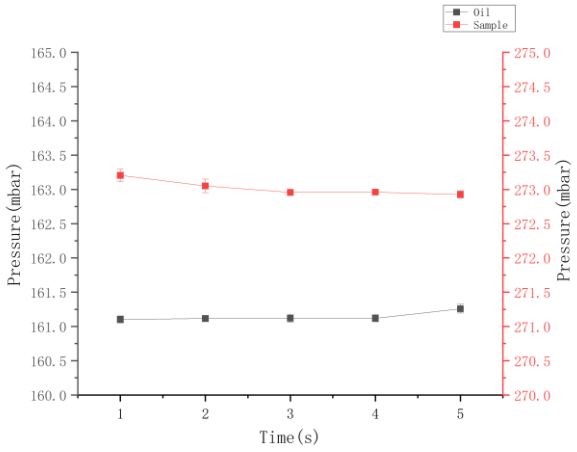

Figure 7. Pressure map during micro droplet generation

In the experiment, the sample will be dispersed into droplets of approximately 50,000 diameters within 3 min while entering the droplet collection chamber following the microchannel under positive pressure and capillary action (Fig. 6 (c)). ImageJ software is adopted to process images captured from experiments. The diameter of the generated droplets can be obtained through experiments after several settings (e.g., the binarization, edge searching, and threshold adjustment). As revealed by the experimental results, the average diameter of the droplets is approximately 87μm. The standard deviation of the average diameter reaches 1.02um, the coefficient of variation (CV%) is nearly 0.91%, and the volume of each droplet is about 0.27nL, confirming that the droplet generation exhibits excellent uniformity and competence in conforming to the needs of biochemical experimental detection and analysis.

3.2. Bubble Suppression During PCR Process

Different pressure values are set in this study in accordance with the theory, 0 mabr, 700 mbar, 1,500 mbar, and 2,000 mbar, and calibrated the device's air pressure by a pressure calibrator. As indicated by the results, the average pressure is 1,504.2 mbar, and it fluctuates within ± 0.2 mbar in 10 min in Fig. 8(a). Next, the generated chip is placed in the device, the PCR process and 40 temperature cycles are set. The Peltier power reaches 120W, which can achieve an average temperature rise and fall rate of 2.5 ℃/s on the surface of the aluminum plate. In the PCR process, 50 ℃, 72 ℃, and 95 ℃ are set, and the temperature on the surface of the aluminum plate over time is presented in Fig. 8(b). As indicated by the results, the deviation between the surface temperature of the aluminum plate and the set temperature is within 0.5 ℃, and the temperature uniformity of six random points on the aluminum plate surface is examined within a scope of 0.5 ℃.

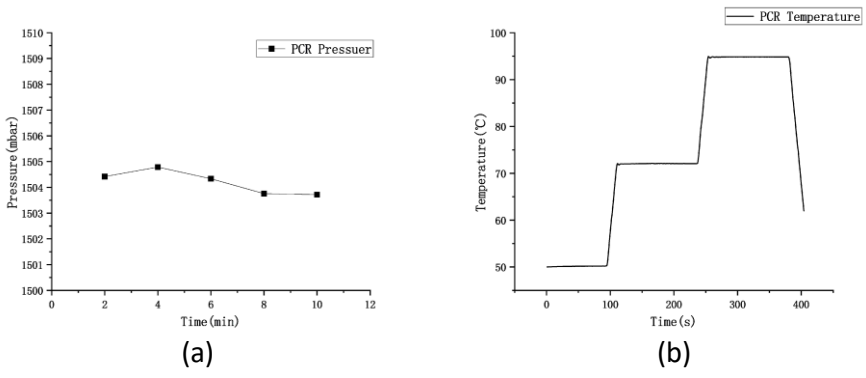

Figure 8. Pressure and temperature map at PCR

Preprints (www.preprints.org) | NOT PEER-REVIEWED | Posted: 30 May 2023 doi:10.20944/preprints202305.2110.v1

During the PCR, the pressure slowly increased to 1,500mabr as the temperature increased. After reaching 1,500mbar, the pressure continued until the end of the PCR process. After completing the PCR process, we continued to maintain it for 5 min, and then slowly reduce the pressure to atmospheric pressure. After ending the pressure continuing, the experimental results are shown in Fig. 9. The results show that the most of the micro droplets inside the chip were destroyed at pressure of 0mabr, and the solution dried up, as shown in Fig. 9. (a). When the pressure was 700mbar, there are large bubbles forming inside the chip, as shown in Fig. 9. (b); when the pressure was 1,500mbar, the micro droplets inside the chip are intact as shown in Fig. 9 (c); when the pressure is 2,000mbar, micro droplets break up inside the chip as shown in Fig. 9 (d). Although micro droplet damage occurred at both 700mbar and 2,000mbar pressures, the reasons for the two are different. Under the pressure of 700 mbar, the formation of larger bubbles is caused by the re-precipitation of gas in the solution; at the pressure of 2,000 mbar, excessive pressure was applied to the cavity, resulting in shear force and damage to the droplets, where no new gas was released and no large bubbles were formed.

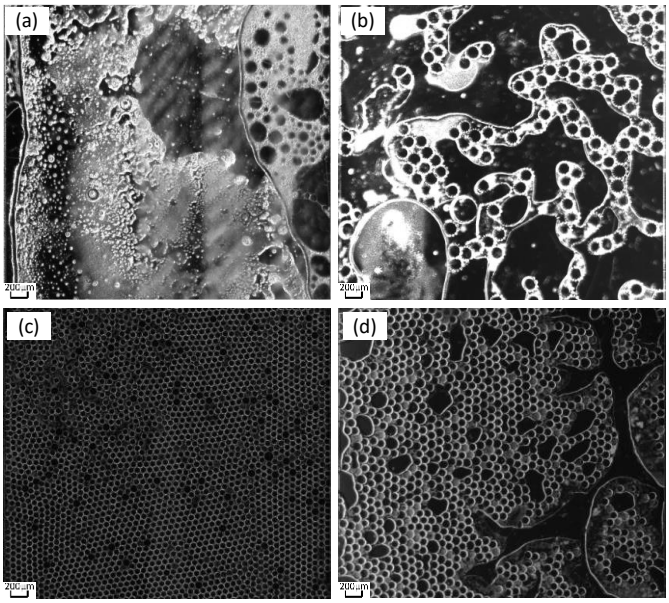

Figure 9. PCR Results under Different Pressures

3.3. Quantitative Testing

The PCR amplified fluorescence signal is examined by transferring the chip to the Laser-induced fluorescence chip reader (Fig. 10). The probe binds to the target gene while releasing a fluorescent reporter. Accordingly, droplets containing templates are capable of observing strong fluorescence signals under excitation light. In contrast, droplets without templates only exhibit weak background fluorescence signals. Thus, fluorescence intensity can be adopted to designate droplets as positive or negative, where the identification and statistics of negative/positive droplets take on critical significance in ddPCR technology. The grayscale values of droplets in fluorescence images are red using ImageJ v4.4 (National Institutes of Health) software, and fluorescence thresholds are determined based on differences in droplet fluorescence intensity. Droplets with fluorescence signals greater than the threshold are considered positive, whereas those below the threshold are considered negative. The quantitative detection of nucleic acid is validated using a constant pressure regulatory device based on ddPCR gene chip in accordance with Poisson's statistical principle. EGFR exon 18 gene serves as the target DNA molecule, and the pGEM plasmid solution of EGFR exon 18 gene is diluted to generate 1×10^{1} to 1×10^{5}copies/ μ concentration gradient standards of five orders of magnitude for L. As depicted in Fig. 11a, the positive droplets are generally saturated when the sample concentration is 10^{5}

Preprints (www.preprints.org) | NOT PEER-REVIEWED | Posted: 30 May 2023 doi:10.20944/preprints202305.2110.v1

copies/micron L. The number of positive droplets is decreased with the template concentration from 10^5 copies /μL to 10^1 copies /μL (Fig. 11b–e).

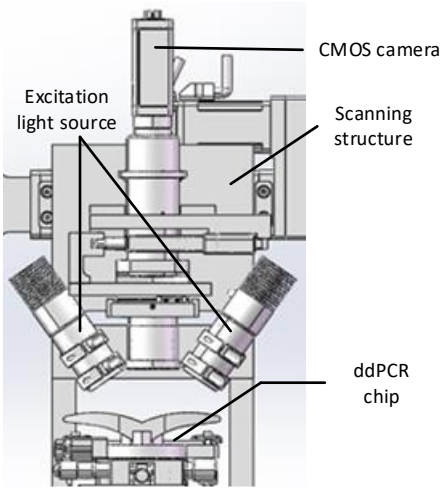

Figure 10. Fluorescence signal acquisition system

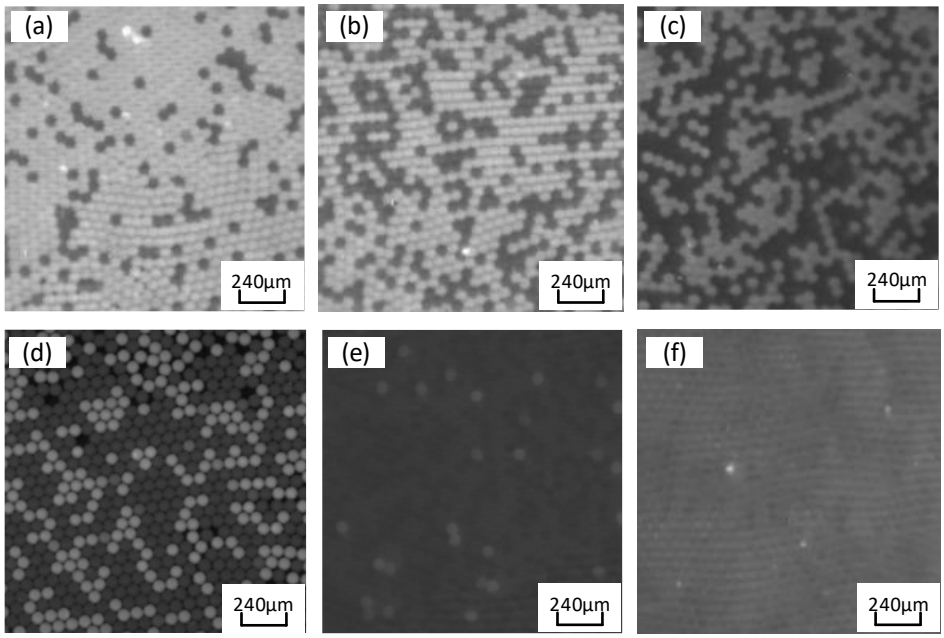

Figure 11. Fluorescence images for simultaneous detection of epidermal growth factor receptor (EGFR) exon18 gene with various DNA concentrations. DNA concentration (copies/μL): a 10^5; b 10^4; c 10^3; d 10^2; e 10^1; f negative control

Preprints (www.preprints.org) | NOT PEER-REVIEWED | Posted: 30 May 2023 doi:10.20944/preprints202305.2110.v1

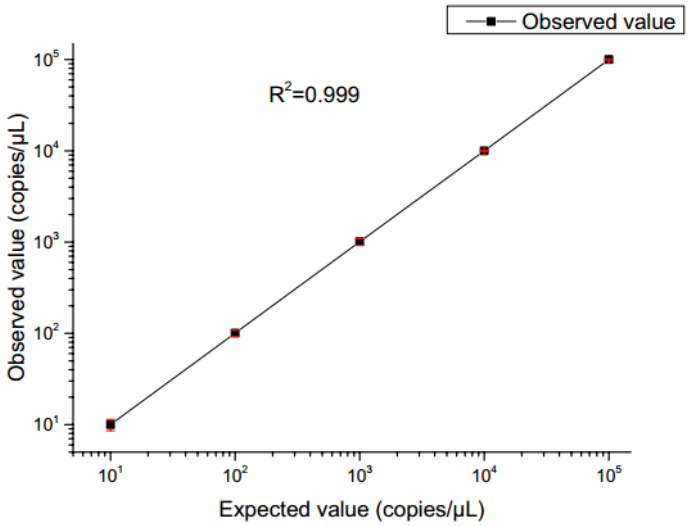

Figure 12. Observed value in the integrated droplet digital polymerase chain reaction (ddPCR) gene chip against the expected value. The error bars represent the 95% confidence interval

The fluorescence images are captured after 40 thermal cycles, and the fluorescence signal is determined via the fluorescence excitation channel of EGFR exon gene 18 with light excitation at 485 nm (FAM). In accordance with Poisson's statistical principle, Eq. (9) is adopted to calculate the absolute amount of target DNA in the respective reaction system. The concentration of DNA templates is calculated based on the results of fluorescence detection systems for samples with different concentration gradients. Subsequently, the standard curve is generated (Fig. 12). After ddPCR gene chip in detecting the target gene concentration of 1×10^1 to 1×10^5 copies /μL is summarized, the results reveal a good linear relationship.

4. Conclusions

The device is developed based on microfluidic chips with micro droplet generation and PCR constant pressure regulation, which achieves droplet generation and PCR amplification on the identical chip, followed by fluorescence detection analysis. Moreover, the source of bubbles and the theory of bubble dynamic behavior in rapid temperature changes are discussed by analyzing the digital PCR process, such that the problem of bubble growth and generation can be solved. The device is highly competent in stably generating micro droplets without bubbles in the chip while performing PCR amplification at 1,500mbar. The amplified micro droplets will not break or mix, supporting subsequent fluorescence detection. Furthermore, the device and integrated ddPCR gene chip are employed to quantitatively detect EGFR exon gene 18 fragments. As revealed by the results, a good linear correlation is generated when the DNA concentration was between 10^1 ~ 10^5 copies/μL in the range. Accordingly, the constant pressure regulation device has promising applications in the field of nucleic acid-associated detection based on microfluidic chips.

Author Contributions: Y.Y. contributed to the conception of the study, X.M. performed the experiment, D.L. contributed data analysis and wrote the manuscript. All authors have read and agreed to the published version of the manuscript.

Funding: This research received no external funding.

Conflicts of Interest: The authors declare no conflict of interest.

References

1. Auroux, P.A.; Koc, Y.; Demello, A.; Manz, A.; Day, P. Miniaturised nucleic acid analysis. *Lab Chip* **2004**, *4*, 534-546.

2. Gingeras, T.R.; Higuchi, R.; Kricka, L.J.; Lo, Y.D.; Wittwer, C.T. Fifty Years of Molecular (DNA/RNA) Diagnostics. *Clinical Chemistry* **2005**, *51*, 661-671.
3. Roper, M.G.; Easley, C.J.; Landers, J.P. Advances in Polymerase Chain Reaction on Microfluidic Chips. *Analytical Chemistry* **2005**, *77*, 3887-3894.
4. Meng, X.; Yu, Y.; Gong, P.; Jin, G. An integrated droplet digital PCR gene chip for absolute quantification of nucleic acid. *Microfluidics and Nanofluidics* **2021**, *25*, 62.
5. Diaz, L.A.; Bardelli, A. Liquid Biopsies: Genotyping Circulating Tumor DNA. *Journal of Clinical Oncology* **2014**, *32*, 579-586.
6. Whale, A.S.; Huggett, J.F.; Simon, C.; Valerie, S.; Jacqui, S.; Stephen, E.; Foy, C.A.; Scott, D.J. Comparison of microfluidic digital PCR and conventional quantitative PCR for measuring copy number variation. *Nucleic Acids Research* **2012**, *40*, e82.
7. Hashimoto-Torii, K.; Torii, M.; Fujimoto, M.; Nakai, A.; El?Fatimy, R.; Mezger, V.; Ju, M.J.; Ishii, S.; Chao, S.H.; Brennand, K.J. Roles of heat shock factor 1 in neuronal response to fetal environmental risks and its relevance to brain disorders. *Neuron* **2014**, *82*, 560-572.
8. Zhong, Q.; Bhattacharya, S.; Kotsopoulos, S.; Olson, J.; Taly, V.; Griffiths, A.D.; Link, D.R.; Larson, J.W. Multiplex digital PCR: breaking the one target per color barrier of quantitative PCRElectronic supplementary information (ESI) available. See DOI: 10.1039/c1lc20126c. *Lab on a Chip - Miniaturisation for Chemistry & Biology* **2011**, 2167-2174.
9. Mu, D.; Yan, L.; Tang, H.; Liao, Y. A sensitive and accurate quantification method for the detection of hepatitis B virus covalently closed circular DNA by the application of a droplet digital polymerase chain reaction amplification system. *Biotechnology Letters* **2015**.
10. Zhang, H.; Jenkins, G.; Zou, Y.; Zhu, Z.; Yang, C.J. Massively Parallel Single-Molecule and Single-Cell Emulsion Reverse Transcription Polymerase Chain Reaction Using Agarose Droplet Microfluidics. *Analytical Chemistry* **2012**, *84*, 3599-3606.
11. Dawson; S-J; Tsui; DWY; Murtaza. Analysis of Circulating Tumor DNA to Monitor Metastatic Breast Cancer. *Breast diseases* **2013**, 1199-1209.
12. Yin, K.; Zeng, X.; Liu, W.; Xue, Y.; Li, X.; Wang, W.; Song, Y.; Zhu, Z.; Yang, C.J. Stable Colloidosomes Formed by Self-Assembly of Colloidal Surfactant for Highly Robust Digital PCR. *Analytical Chemistry* **2019**, 6003-6011.
13. Bian, X.; Jing, F.; Li, G.; Fan, X.; Jia, C.; Zhou, H.; Jin, Q.; Zhao, J. A microfluidic droplet digital PCR for simultaneous detection of pathogenic Escherichia coli O157 and Listeria monocytogenes. *Biosensors & Bioelectronics* **2015**, 770-777.
14. Xu, J.; Vaillant, R.; Attinger, D. Use of a porous membrane for gas bubble removal in microfluidic channels: physical mechanisms and design criteria. *Microfluidics and Nanofluidics* **2010**, *9*, 765-772.
15. Nakayama, T.; Kurosawa, Y.; Furui, S.; Kerman, K.; Kobayashi, M.; Rao, S.R.; Yonezawa, Y.; Nakano, K.; Hino, A.; Yamamura, S. Circumventing air bubbles in microfluidic systems and quantitative continuous-flow PCR applications. *Analytical and Bioanalytical Chemistry* **2006**, *386*, 1327-1333.
16. Liu, H.B.; Gong, H.Q.; Ramalingam, N.; Jiang, Y.; Dai, C.C.; Hui, K.M. Micro air bubble formation and its control during polymerase chain reaction (PCR) in polydimethylsiloxane (PDMS) microreactors. *Journal of Micromechanics & Microengineering* **2007**, *17*, 2055.
17. Schuler, F.; Trotter, M.; Geltman, M.; Schwemmer, F.; Wadle, S.; Domínguez-Garrido, E.; López, M.; Cervera-Acedo, C.; Santibáez, P.; Stetten, F.v. Digital droplet PCR on disk. *Lab Chip* **2016**, *16*, 208-216.
18. Nakayama, T.; Hiep, H.M.; Furui, S.; Yonezawa, Y.; Saito, M.; Takamura, Y.; Tamiya, E. An optimal design method for preventing air bubbles in high-temperature microfluidic devices. *ANALYTICAL AND BIOANALYTICAL CHEMISTRY* **2010**, 457-464.
19. Karlsson, J.M.; Haraldsson, T.; Laakso, S.; Virtanen, A.; Maki, M.; Ronan, G.; Wijngaart, W. *PCR on a PDMS-based microchip with integrated bubble removal*. in *Solid-state Sensors, Actuators & Microsystems Conference*. 2011.
20. Ciardiello, F.; Tortora, G. EGFR antagonists in cancer treatment. *N Engl J Med* **2008**, *358*, 1160-1174.
21. Jin, G. Numerical Simulation and Experimental Verification of Droplet Generation in Microfluidic Digital PCR Chip. *Micromachines* **2021**, *12*, 409.
22. Chen, H.; Cornwell, J.; Zhang, H.; Lim, T.; Resurreccion, R.; Port, T.; Rosengarten, G.; Nordon, R.E. Cardiac-like flow generator for long-term imaging of endothelial cell responses to circulatory pulsatile flow at microscale. *Lab Chip* **2013**, *13*, 2999-3007.
23. Chen, H.; Li, J.; Zhang, H.; Li, M.; Rosengarten, G.; Nordon, R.E. Microwell perfusion array for high-throughput, long-term imaging of clonal growth. *Biomicrofluidics* **2011**, *5*, 345.
24. Hoda, I.; Han, Z.; Anhong, Z. A novel three-dimensional microTAS chip for ultra-selective single base mismatched Cryptosporidium DNA biosensor. **2018**.
25. Zhang, H.; Xiao, L.; Li, Q.; Qi, X.; Zhou, A. Microfluidic chip for non-invasive analysis of tumor cells interaction with anti-cancer drug doxorubicin by AFM and Raman spectroscopy. *Biomicrofluidics* **2018**, *12*, 024119.
26. Fan; Yuanyuan; Dong; Defang; Li; Qingling; Si; Haibin; Pei; Haimeng. Fluorescent analysis of bioactive molecules in single cells based on microfluidic chips. *Lab on a chip* **2018**.
27. Ping; Wang; Fengxiang; Jing; Gang; Li; Zhenhua; Wu; Zule; Cheng. Absolute quantification of lung cancer related microRNA by droplet digital PCR. *Biosensors & bioelectronics* **2015**.